CrossMark

ORIGINAL ARTICLE

Characterization of Rebound Depolarization in Neurons of the Rat Medial Geniculate Body *In Vitro*

Xin-Xing Wang[1] · Yan Jin[2] · Hui Sun[3] · Chunlei Ma[3] · Jinsheng Zhang[4] · Ming Wang[1,2] · Lin Chen[1,2]

Abstract Rebound depolarization (RD) is a response to the offset from hyperpolarization of the neuronal membrane potential and is an important mechanism for the synaptic processing of inhibitory signals. In the present study, we characterized RD in neurons of the rat medial geniculate body (MGB), a nucleus of the auditory thalamus, using whole-cell patch-clamp and brain slices. RD was proportional in strength to the duration and magnitude of the hyperpolarization; was effectively blocked by Ni^{2+} or Mibefradil; and was depressed when the resting membrane potential was hyperpolarized by blocking hyperpolarization-activated cyclic nucleotide-gated (HCN) channels with ZD7288 or by activating G-protein-gated inwardly-rectifying K^+ (GIRK) channels with baclofen. Our results demonstrated that RD in MGB neurons, which is carried by T-type Ca^{2+} channels, is critically regulated by HCN channels and likely by GIRK channels.

✉ Lin Chen
linchen@ustc.edu.cn

[1] CAS Key Laboratory of Brain Function and Diseases, School of Life Sciences, University of Science and Technology of China, Hefei 230027, China

[2] Auditory Research Laboratory, School of Life Sciences, University of Science and Technology of China, Hefei 230027, China

[3] Department of Physiology, Binzhou Medical University, Yantai 264003, China

[4] Department of Otolaryngology - Head and Neck Surgery, Wayne State University School of Medicine, Detroit, MI 48201, USA

Introduction

Neuronal rebound depolarization (RD) is a voltage response to the offset from hyperpolarization of the membrane potential [1, 2] and often results in the firing of action potentials when sufficiently robust. RD can be evoked by inhibitory synaptic stimuli *in vivo* [3] or hyperpolarizing current injection *in vitro* [4, 5]. In the central auditory system, RD has been recorded in the inferior colliculus [6], superior paraolivary nucleus [7, 8], thalamic reticular nucleus [9] and medial geniculate body (MGB) [10, 11]. RD has important functional implications in auditory information-processing. In the superior paraolivary nucleus, RD is known to be involved in encoding sound rhythms [7]. In the inferior colliculus, RD has been proposed to play an important role in encoding features of sounds, including duration and temporal selectivity [12, 13].

The MGB is an important nucleus of the auditory thalamus. In the rat MGB, 99% of the neurons are glutamatergic [14, 15] and receive inhibitory inputs mainly from the inferior colliculus and the thalamic reticular nucleus [16–20]. The inhibitory inputs are distributed across the dorsal and ventral parts of the MGB and evoke inhibitory postsynaptic potentials [16, 21] which can hyperpolarize an MGB neuron sufficiently to produce a robust RD [22–24]. Although RD is a prominent feature of MGB neurons [4, 5], its detailed physiological characteristics have not been described. The purpose of the present study was to

characterize RD using the whole-cell patch-clamp recording technique in brain slices.

Materials and Methods

Animals

Wistar rats (aged 15–22 days, male or female) were used. All procedures were approved by the Animal Care and Use Committee at the University of Science and Technology of China. Slices containing the MGB were prepared using a procedure similar to that described previously [21, 25]. Briefly, the rat was decapitated and the brain was rapidly removed and submerged in ice-cold artificial cerebrospinal fluid (ACSF) containing (in mmol/L) 129 NaCl, 3 KCl, 1.2 KH_2PO_4, 1.3 $MgSO_4$, 20 $NaHCO_3$, 2.4 $CaCl_2$, 3 HEPES, and 10 *D*-glucose at pH 7.3–7.4 (osmolarity: 300–310 mOsm/kg). The ACSF was continuously bubbled with 95% O_2 and 5% CO_2. The caudal portion of the cerebrum, embracing the right and left hemispheres, was separated by two coronal cuts in the midbrain and the forebrain. The brain was sectioned in the horizontal plane into 300-μm slices using a vibrating microtome (DTK-1000, Dosaka, Kyoto, Japan). The slices were immersed in oxygenated ACSF in a holding chamber for at least 1 h at 28 °C before electrophysiological recording.

Whole-Cell Patch-Clamp Recording

Slices containing the MGB were transferred from the holding chamber to a recording chamber (TC-344B, Middlesex County, MA), in which oxygenated ACSF at 34 °C was circulated at 3 mL/min. MGB neurons were visualized under an upright microscope (FN1; Nikon, Tokyo, Japan) equipped with a digital CCD camera using a 40× water-immersion objective (FN1, Nikon) and infrared-differential interference optics (Fig. 1B). For whole-cell patch-clamp recording, we used an HEKA EPC-9 amplifier and PatchMaster software (HEKA Electronics, Lambrecht (Pfalz), Germany). Signals were filtered at 2.9 kHz and digitized at 10 kHz. Electrodes for whole-cell patch-clamp recording were prepared from borosilicate capillaries with a two-stage vertical puller (PC-10, Narishige, Tokyo, Japan). The electrode was filled with internal solution containing (in mmol/L): 130 K-gluconate, 2 $MgCl_2$, 5 KCl, 0.6 EGTA, 10 HEPES, 2 Mg-ATP, and 0.3 Na-GTP. The pH was adjusted to 7.2–7.4 with KOH (1 mol/L) and the osmolarity was 280–300 mOsm/kg. The resistance of patch electrodes was 4–6 MΩ. The liquid junction potential was calculated at $\sim$15 mV and was not corrected. RD was evoked by a hyperpolarizing step current in current-clamp recording mode. Unless otherwise indicated, tetrodotoxin (TTX; 1 μmol/L) was added to the bath to eliminate rebound spikes and facilitate the measurement of RD properties. The location of neurons under recording relative to MGB divisions was visually identified by referring to the Paxinos and Watson atlas (4th edition).

Pharmacology

Mibefradil was prepared at a stock concentration of 3 mmol/L and stored at −20 °C. It was used within 3 months and diluted to a final concentration from 3 to 10 μmol/L on use. When $NiCl_2$ (100 μmol/L) was applied, KH_2PO_4 was not added to the ACSF to prevent precipitation. $BaCl_2$ (100 mmol/L), $NiCl_2$ (100 mmol/L), baclofen (3 mmol/L), Tertiapin-Q (200 μmol/L), TTX (1 mmol/L), and 4-ethylphenylamino-1,2-dimethyl-6-methylaminopyrimidinium chloride (ZD7288; 50 mmol/L) were prepared as stock solutions (×1000) and diluted in ACSF on use. All drugs were from Sigma-Aldrich Inc., (St. Louis, MO), except TTX (Hebei Aquatic Science and Technology Development Co., Qinhuangdao, China) and Tertiapin-Q (Tocris Cookson, Bristol, UK).
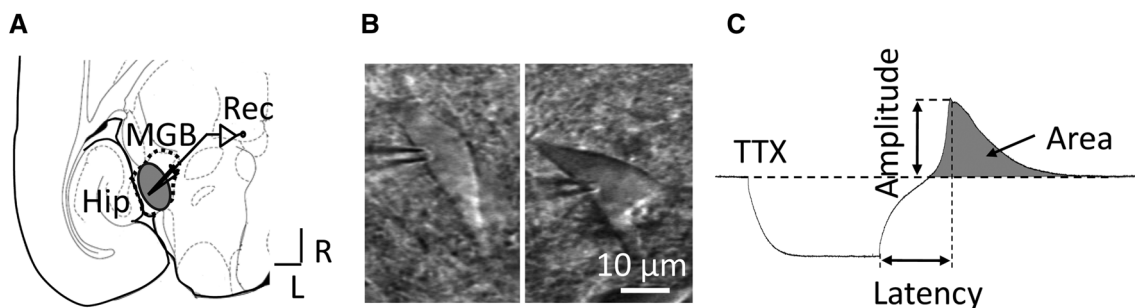

Fig. 1 A Schematic of a horizontal slice containing the MGB, **B**, **C** Two sample MGB neurons viewed under a differential interference contrast microscope (**B**) and a representative example of RD showing how its amplitude, latency, and area were measured (**C**). R, rostral; L, lateral; MGB, medial geniculate body; Hip, hippocampus; Rec, site of patch clamp recording; TTX, tetrodotoxin; RD, rebound depolarization.

Data Analysis

Quantitative characterization of the RD properties amplitude, area, peak latency, and rise slope was similar to that described previously (Fig. 1C) [6, 7]. The RD amplitude was defined as the peak voltage over the resting membrane potential and the latency as the time from the release of hyperpolarization to the peak of RD. All the amplitudes over the resting membrane potential were defined as the RD area (Fig. 1C). The rise slope of the RD was measured between 10% and 90% of the peak amplitude. All analyses and figures were made using Clampfit 10.0 (Axon, Sunnyvale, CA) and OriginPro 8.0 (Origin Lab, Northampton, MA). All data are presented as mean $\pm$ SE. Student's t test (paired, one-tailed) was used for analysis of the effects of adjusting the resting membrane potential. One-way or two-way repeated measures analysis of variance (RM-ANOVA) with Bonferroni correction was used to analyze differences within groups. If two-way RM-ANOVA resulted in a significant main effect or a significant interaction, a one-way RM-ANOVA with Bonferroni correction was performed for pairwise comparisons. $P < 0.05$ was considered statistically significant. Pearson's correlation was used to determine whether the correlation between RD properties and another variable was significant.

Results

The Strength of RD was Proportional to the Magnitude and Duration of Hyperpolarization

The neurons from which we recorded were from the ventral and dorsal parts of the MGB (elliptical region in Fig. 1A). None of the neurons with a stable resting membrane potential (V_{rest}; more negative than -52 mV) fired spontaneously. There was no significant difference in the V_{rest} between neurons in the ventral and dorsal MGB (dorsal: -59.06 ± 0.56 mV, $n = 36$; ventral: -58.41 ± 0.74 mV, $n = 22$, $P > 0.05$), which is consistent with the findings of Bartlett and Smith [5]. Action potentials were evoked by a robust RD (Fig. 2A). In most cases, an MGB neuron exhibited various patterns of rebound discharge ranging from a single spike to complex firing following strong hyperpolarization (Fig. 2A). These spikes were eliminated by 1 μmol/L TTX and only five neurons (3.18%, 5/157 cells) in the presence of TTX still showed a rebound spike, which was presumably a high-threshold activated Ca^{2+} spike (Fig. 2B) [10].

We quantitatively characterized RD in response to hyperpolarizing currents of various magnitudes and durations and found that the strength of RD was proportional to the magnitude and duration of hyperpolarization within a certain range. With a hyperpolarizing current 205 ms in duration, the normalized RD amplitude gradually increased from $54.71 \pm 15.08\%$ to $96.78 \pm 2.64\%$ (Pearson: $r = -0.79$, $n = 18$, $P < 0.01$) and the normalized RD area from $48.45 \pm 10.91\%$ to $85.53 \pm 3.01\%$ (Pearson: $r = -0.74$, $n = 18$, $P < 0.01$) as the current magnitude increased from -40 to -300 pA (Fig. 3A, C, and E). In contrast, the normalized RD latency decreased from $274.60 \pm 26.37\%$ to $123.87 \pm 7.51\%$ (Pearson: $r = 0.61$, $n = 18$, $P < 0.01$) (Fig. 3A, C, and E). When the injected current was -40 pA, the normalized RD amplitude gradually increased from $3.57 \pm 1.11\%$ to $94.03 \pm 6.35\%$ (Pearson: $r = 0.91$, $n = 34$, $P < 0.01$) and the normalized RD area from $0.10 \pm 1.47\%$ to $95.68 \pm 11.13\%$ (Pearson: $r = 0.92$, $n = 34$, $P < 0.01$) as the current duration increased from 25 to 685 ms (Fig. 3B, D, and E). In contrast, the normalized RD latency decreased from $455.39 \pm 61.00\%$ to $202.84 \pm 14.23\%$ (Pearson: $r = -0.84$, $n = 34$, $P < 0.01$) (Fig. 3B, D, and E). However, the amplitude, area and latency reached a plateau when the magnitude or duration of hyperpolarization was large enough (Fig. 3C–E). Under these experimental conditions, most MGB neurons (76.43%) had RD with amplitudes ranging from 25 to 35 mV (Fig. 2C).

RD Was Blocked by Ni^{2+} or Mibefradil

To confirm the ionic basis of RD in MGB neurons, we tested the actions of Ni^{2+} and Mibefradil, blockers of low-voltage-activated (T-type) Ca^{2+} channels. Ni^{2+} almost eliminated RD as shown by the dramatic drop in RD amplitude (29.24 ± 1.04 vs 3.68 ± 0.67 mV, $n = 10$, $P < 0.01$), the drop in RD area (2.23 ± 0.17 vs 0.49 ± 0.12 mV∗s, $n = 10$, $P < 0.01$) and the increase in RD latency (80.55 ± 8.32 vs 286.77 ± 33.12 ms, $n = 10$, $P < 0.01$) following its application (Fig. 4A, B).

Mibefradil, a specific blocker of T-type Ca^{2+} channels, had a similar inhibitory effect on RD as shown by the drop in amplitude (30.24 ± 1.06 vs 6.22 ± 1.03 mV, $n = 16$, $P < 0.01$) and area (2.96 ± 0.21 vs 0.69 ± 0.10 mV∗s, $n = 16$, $P < 0.01$), and the increase in latency (143.76 ± 14.17 vs 283.86 ± 29.66 ms, $n = 16$, $P < 0.01$) following its application (Fig. 4C, D). The blocking effects of Ni^{2+} and Mibefradil indicated that the RD in MGB neurons is carried by T-type Ca^{2+} channels.

RD Was Depressed by ZD7288

We showed that 50 μmol/L ZD7288 blocked the hyperpolarization-activated cyclic nucleotide-gated (HCN) channels in MGB neurons (Fig. S1). The blockade of HCN channels depressed the RD (Fig. 5A). With a hyperpolarizing current at -80 pA, ZD7288 decreased the RD
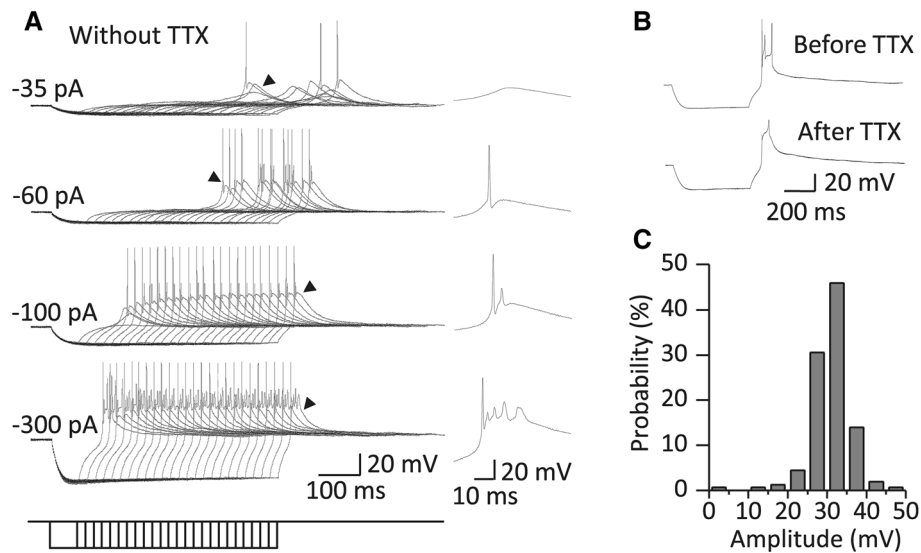
Fig. 2 Robust RD was evoked from most MGB neurons. **A** Left panels; sample traces of the RD recorded from an MGB neuron in response to a series of hyperpolarizing currents with durations from 65 to 565 ms (20 ms/step). Note that the RD was robust enough to trigger rebound firing in the absence of TTX. Arrowheads indicate representative firing patterns that are expanded in the right panels.

B Sample traces of RD recorded from another MGB neuron showing that TTX did not completely block the rebound firing in a rare circumstance. RD was evoked by a 500-ms hyperpolarizing current at -80 pA. **C** Amplitude distribution of RD ($n = 157$) in response to a 500-ms hyperpolarizing current at -100 pA ($n = 89$) or to a 200-ms current at -140 pA ($n = 68$).

amplitude from $97.41 \pm 1.10\%$ to $48.60 \pm 9.53\%$ ($P < 0.01$), decreased the area from $94.21 \pm 1.52\%$ to $56.29 \pm 11.14\%$ ($P < 0.01$), decreased the rise slope from $104.21 \pm 5.75\%$ to $63.29 \pm 13.66\%$ ($P < 0.05$), and increased the latency to the peak from $108.71 \pm 1.80\%$ to $361.35 \pm 45.91\%$ ($P < 0.01$) ($n = 25$, Fig. 5B).

The blockade of HCN channels also hyperpolarized the V_{rest} (-57.92 ± 0.71 *vs* -63.38 ± 1.03 mV, $n = 25$, $P < 0.01$) (Fig. 5D) and increased the input resistance (372.94 ± 20.05 *vs* 435.15 ± 30.86 MΩ, $n = 25$, $P < 0.05$) (Figs. 5E and S2A). Because the ZD7288-induced depression of the RD was significantly correlated with the ZD7288-induced hyperpolarization of V_{rest} (Fig. S3A–C), we investigated whether RD was suppressed by the hyperpolarized V_{rest}. We found that the regulatory effects of ZD7288 on RD properties (except the latency) were reversed when the otherwise hyperpolarized membrane potential by ZD7288 was adjusted back to the control level by injecting positive current (Fig. 5A, C). Our data indicated that HCN channels regulate RD properties mainly through changing the V_{rest}.

RD Was Regulated by Ba^{2+}

Inwardly rectifying potassium (Kir) channels play an important role in maintaining the normal V_{rest} of neurons [26]. Ba^{2+} at micromolar concentrations is a relatively specific blocker of Kir channels [27, 28]. We found that 100 μmol/L Ba^{2+} depolarized the V_{rest} from -58.66 ± 0.62 to -54.12 ± 0.66 mV ($n = 31$, $P < 0.01$)

(Fig. 6D) and increased the input resistance from 394.94 ± 29.95 to 466.04 ± 50.33 MΩ ($n = 18$, $P < 0.01$) (Figs. 6E and S3B) in MGB neurons. Since RD was sensitive to the V_{rest} (Fig. 5C), we then investigated the role of Kir channels in the regulation of RD.

We found that blockade of Kir channels by Ba^{2+} significantly changed the properties of RD in MGB neurons (Fig. 6A and B). With a hyperpolarizing current at -80 pA, application of Ba^{2+} decreased the amplitude ($98.29 \pm 1.49\%$ *vs* $90.45 \pm 1.72\%$, $P < 0.01$) and the latency to the peak ($106.14 \pm 1.38\%$ *vs* $81.11 \pm 3.10\%$, $P < 0.01$), but increased the area ($93.47 \pm 3.07\%$ *vs* $106.71 \pm 4.55\%$, $P < 0.05$) and the rise slope ($92.02 \pm 2.26\%$ *vs* $203.37 \pm 23.67\%$, $P < 0.01$) ($n = 27$, Fig. 6B). Moreover, the area, rise slope and latency of RD were significantly correlated with Ba^{2+}-induced depolarization of the V_{rest} (Fig. S4A–C).

We found that the regulatory effects of Ba^{2+} on the amplitude and rise slope of RD were reversed if the otherwise depolarized membrane potential was adjusted back to the control level by injecting a negative current (Fig. 6A, C). However, the area and the latency to the peak of RD did not fully recover when the membrane potential was adjusted back to the control level.

Activation of G-Protein-Gated Kir Channels Depressed the RD

We then investigated the role of G-protein-gated Kir (GIRK) channels, a subfamily of Kir channels, in RD. The

Fig. 3 Properties of RD in response to hyperpolarizing currents of various durations and strengths. **A** Voltage responses recorded from an MGB neuron to a series of 200-ms hyperpolarizing currents of various strengths from −20 to −140 pA at −20 pA/step. Arrow indicates a graded RD induced by the current at −40 pA. **B** Responses from the same neuron as in **A** to a series of hyperpolarizing currents at −40 pA of various durations from 165 to 665 ms. Note that the RD amplitude only slightly increased with current durations longer than 365 ms (arrow). **C** Typical properties of RD recorded from an MGB neuron as a function of the strength of the hyperpolarizing current with a constant duration (205 ms). **D** Typical properties of RD recorded from an MGB neuron as a function of the duration of the hyperpolarizing current with a constant magnitude (−100 pA). **E** Average values for normalized properties of RD as a function of the magnitude and duration of the hyperpolarizing current ($n = 7$). The measurements are normalized to those of the RD evoked by a 605-ms current at −200 pA.
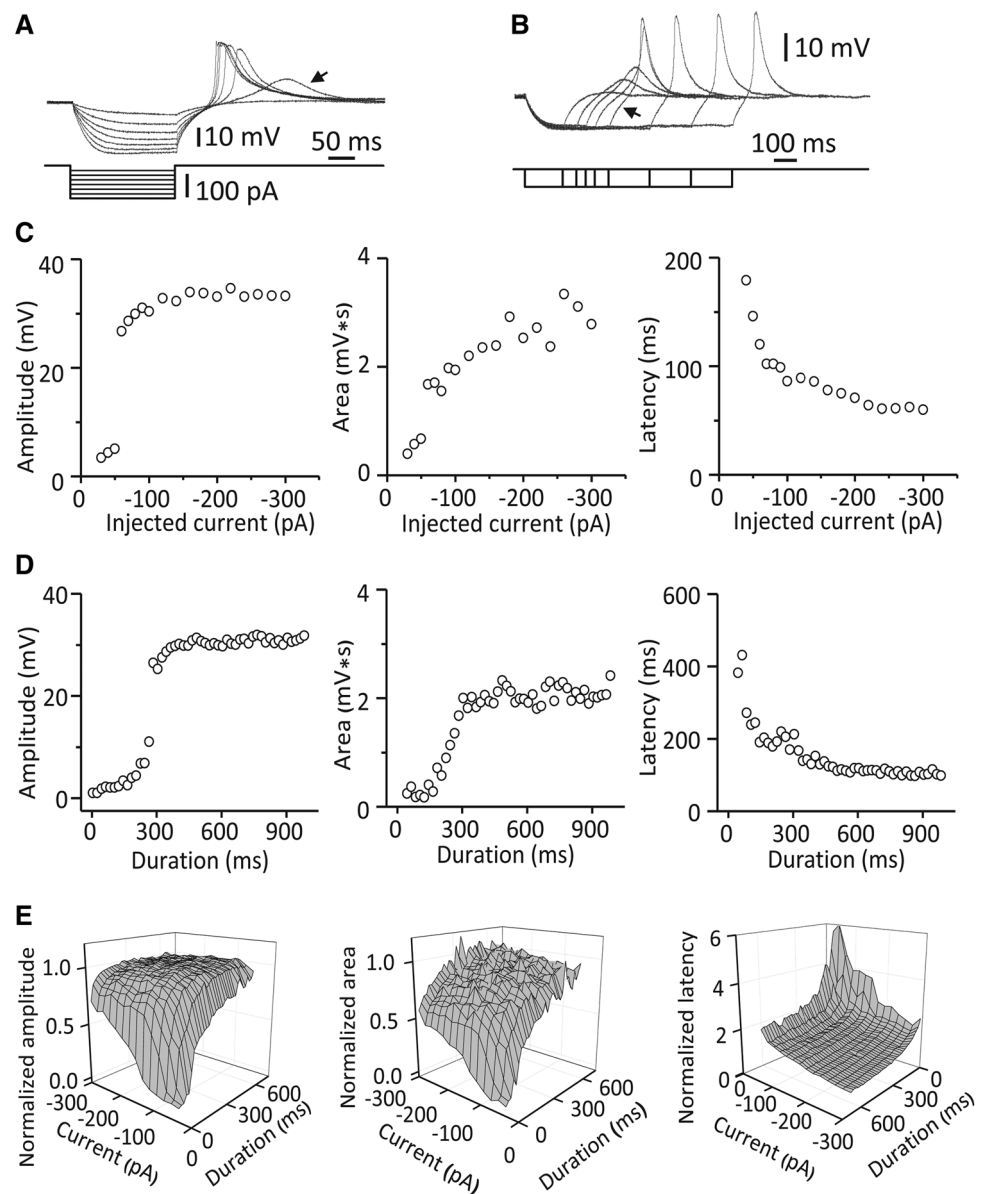
γ-aminobutyric acid B (GABA$_B$) receptor, which is expressed abundantly in MGB neurons [26, 29], activates GIRK channels through the intracellular G-protein pathway [30]. We found that the GABA$_B$ receptor agonist baclofen drastically depressed RD (Fig. 7). With a hyperpolarizing current at −120 pA, baclofen decreased the amplitude (96.73 ± 1.22% vs 10.68 ± 5.75%, $P < 0.01$), the area (93.87 ± 4.41% vs 7.53 ± 3.21%, $P < 0.01$) and the rise slope (94.34 ± 4.23% vs 8.46 ± 3.86%, $P < 0.01$). Baclofen also increased the latency to peak (104.88 ± 1.61% vs 361.45 ± 52.48%, $P < 0.01$) ($n = 10$, Fig. 7B). These effects were reversed to a large extent by Tertiapin-Q (200 nmol/L), a GIRK channel blocker, indicating that the activation of GIRK channels depresses RD (Fig. 7).

Discussion

In the present study, we demonstrated that RD in the MGB is robust and is carried by T-type Ca^{2+} channels (Figs. 2, 4). The magnitude, time course, and kinetics of RD were proportional in strength to the magnitude and duration of hyperpolarization (Fig. 3). Novel findings are that HCN channels (Fig. 5), and likely GIRK channels (Fig. 7), regulate RD mainly by changing the V_{rest}.

RD in MGB Neurons is Carried by T-type Ca^{2+} Channels

We demonstrated that RD in MGB neurons is mediated by T-type Ca^{2+} channels because RD was almost completely

Fig. 4 RD in MGB neurons
was sensitive to blockers of
T-type Ca^{2+} channels.
A Sample traces of RD recorded
from an MGB neuron and
B group data for RD properties
($n = 10$) before (Ctrl) and after
addition of Ni^{2+}. **C** Sample
traces of RD recorded from
another MGB neuron and
D group data for RD properties
($n = 16$) before (Ctrl) and after
addition of Mibefradil. RD was
evoked by a series of
hyperpolarizing currents at
various strengths from -20 to
-140 pA at -20 pA/step and
with a constant duration of
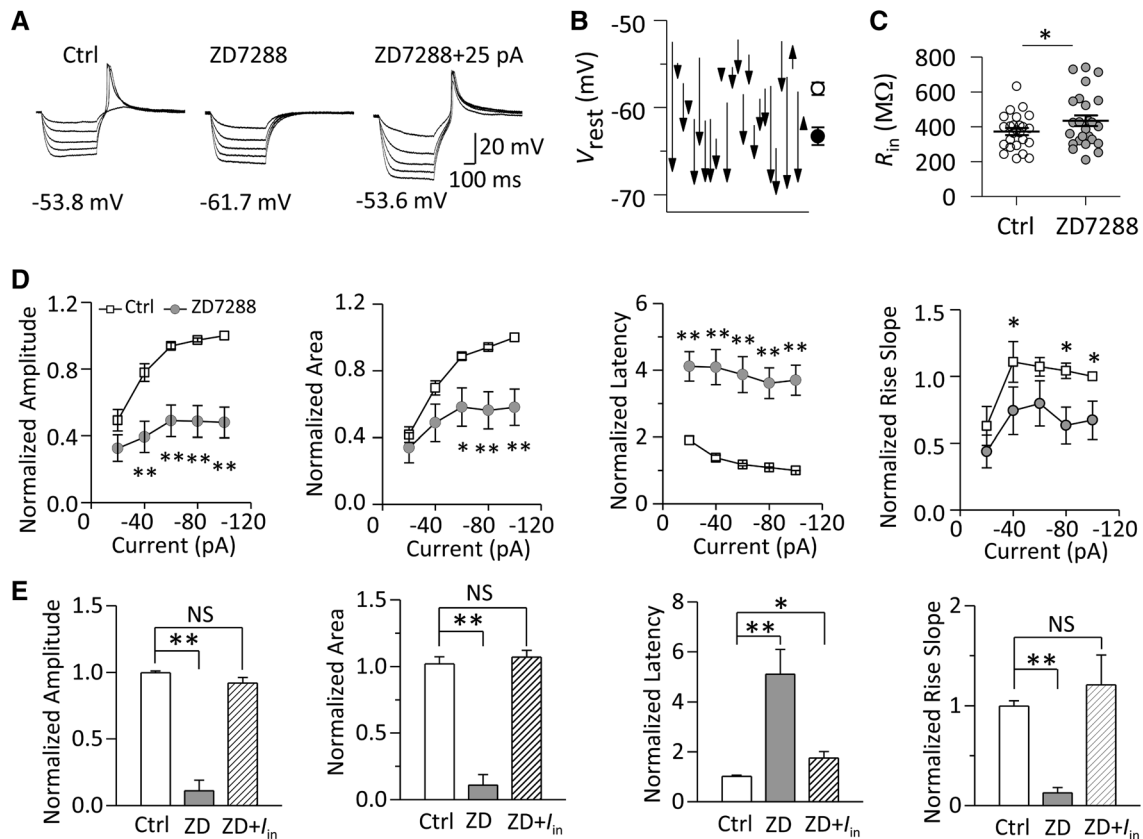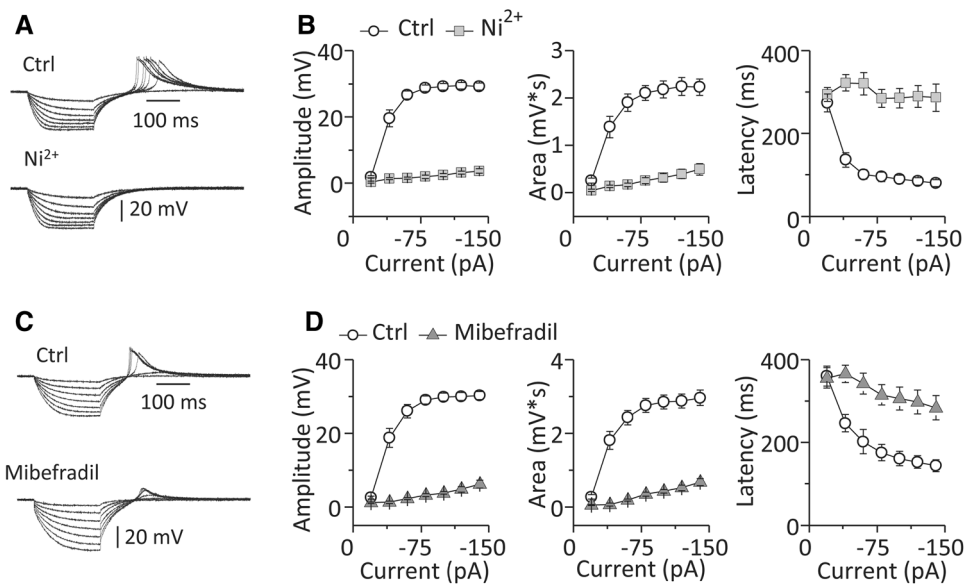200 ms. Vertical bars indicate
standard error.

Fig. 5 Inhibitory effects of the HCN channel blocker ZD7288
(50 μmol/L) on RD. **A** Sample traces of RD recorded from an
MGB neuron. **B**, **C** Group data ($n = 25$) for the normalized
properties of RD (normalized to the values evoked at -100 pA) (**B**) in
response to a series of hyperpolarizing currents (range: -20 to -100
pA at -20 pA/step; duration: 500 ms), and those of the RD ($n = 5$)
(normalized to the values evoked at -120 pA) in response to a
hyperpolarizing current at -100 pA (**C**) in the presence and the
absence (Ctrl) of ZD7288. **D**, **E** Application of ZD7288 also
hyperpolarized the V_{rest} (**D**) and decreased the R_{in} (**E**). V_{rest} indicated
below the traces. I_{in} represents the injected current compensating for
the shifted V_{rest} by ZD7288. $**P < 0.01$, $*P < 0.05$, NS $P > 0.05$.
Vertical bars indicate standard error. V_{rest}, resting membrane poten-
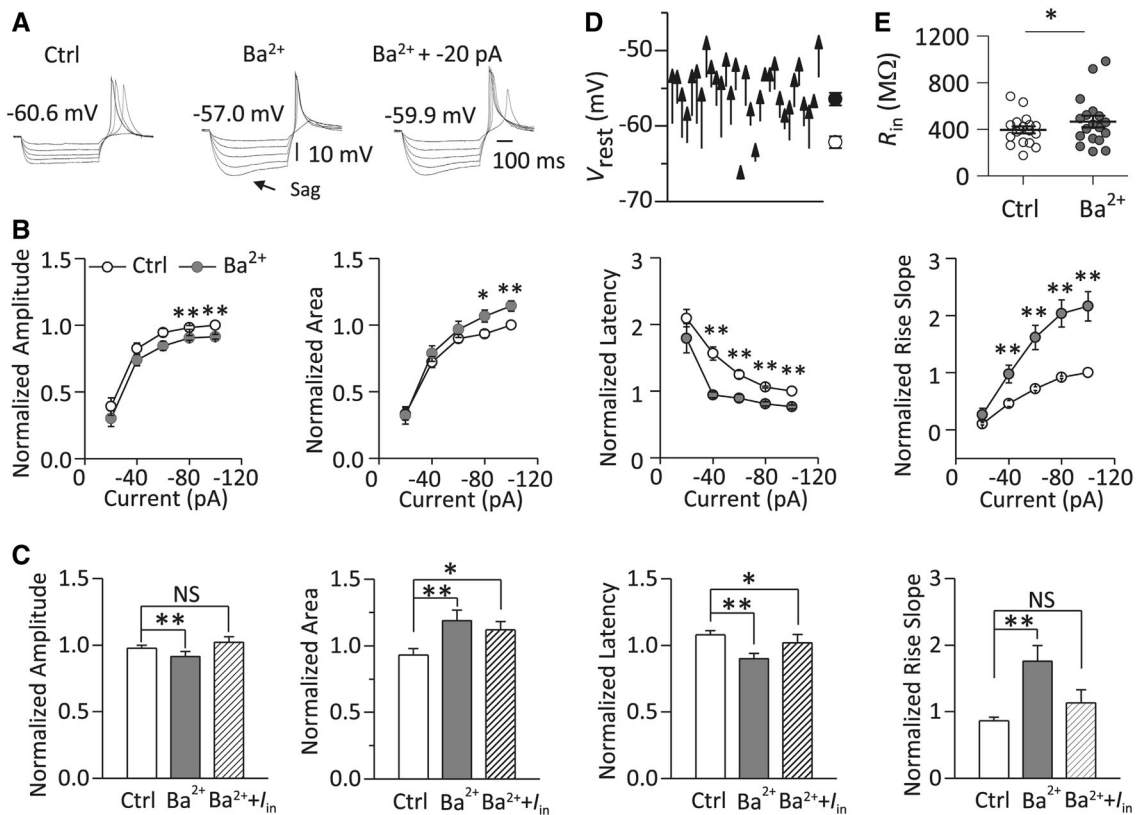tial; R_{in}, input resistance.

Fig. 6 Regulatory effects of the Kir channel blocker Ba^{2+} (100 µmol/L) on RD. **A–C** Sample traces of RD recorded from an MGB neuron (**A**), group data ($n = 27$) for normalized properties of RD (normalized to the values evoked at -100 pA) (**B**) in response to a series of hyperpolarizing currents (range: -20 to -100 pA at -20 pA/step; duration: 500 ms) and those of RD ($n = 9$) (normalized to

the values evoked at -140 pA) in response to a hyperpolarizing current at -100 pA (**C**) in the presence and absence (Ctrl) of Ba^{2+}. **D, E** Application of Ba^{2+} also depolarized the V_{rest} (**D**) and increased the R_{in} (**E**). V_{rest} indicated above the traces. I_{in} represents the injected current to compensate for the shifted V_{rest} by Ba^{2+}. **$P < 0.01$, *$P < 0.05$, NS $P > 0.05$. Vertical bars indicate standard error.
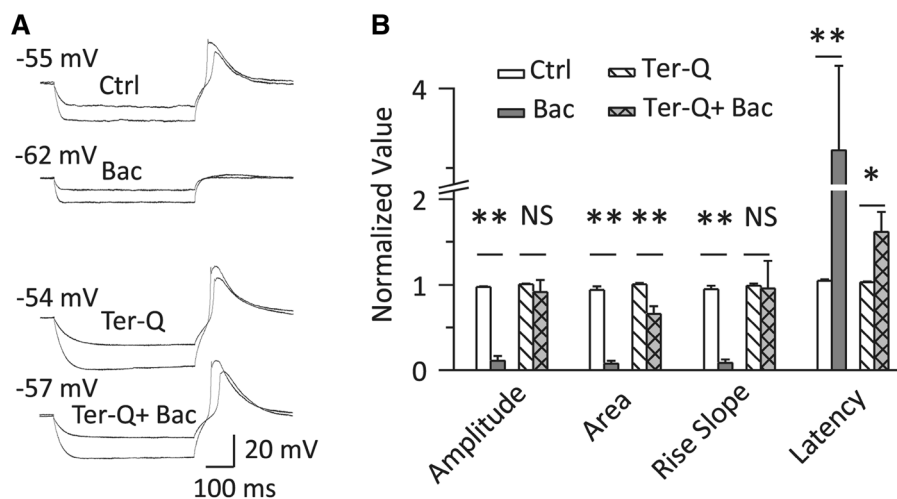

Fig. 7 Activation of GIRK channels depressed RD. **A, B** Sample traces recorded from an MGB neuron (**A**) and group data for RD properties ($n = 10$) showing that baclofen (1.5 µmol/L) depressed RD, but failed to do so when co-applied with Tertiapin-Q (200 nmol/L). The RD traces in (**A**) were evoked by two hyperpolarizing currents at -60 pA and -140 pA for 500 ms. The RD in (**B**) was

evoked by a 500-ms hyperpolarizing current at -120 pA; the measurements of its properties were normalized to those of RD evoked at -140 pA. **$P < 0.01$, *$P < 0.05$, NS $P > 0.05$. Vertical bars indicate standard error. Bac, baclofen; GIRK channel, G-protein-gated inwardly-rectifying K^+ channel; Ter-Q, Tertiapin-Q.

blocked by Ni^{2+} or Mibefradil, blockers of T-type Ca^{2+} channels (Fig. 4). This finding is consistent with previous studies in other brain areas, including the hippocampus [31], inferior colliculus [6], cerebellum [32, 33], and superior paraolivary nucleus [7, 8]. The detailed mechanism underlying RD generation is associated with the unique kinetics of T-type Ca^{2+} channels (Fig. 8). When an MGB neuron is at the V_{rest}, a large portion of T-type Ca^{2+} channels are in an inactivated state [34–36]. When a neuron is conditioned by a hyperpolarizing current, these channels are de-inactivated and ready for activation. Following the offset of hyperpolarization, the recovery of the membrane potential from the hyperpolarized state to the resting state activates T-type Ca^{2+} channels to cause a depolarizing overshoot above the V_{rest}, namely RD.

The characteristic profiles of RD in the MGB are shaped by the kinetics, expression, and development of T-type Ca^{2+} channels. First, a hyperpolarizing current with a longer duration and larger magnitude de-inactivated more T-type Ca^{2+} channels. As a result, the RD was proportional to the duration and magnitude of the hyperpolarizing current (Fig. 3). Second, RD was robust with a mean amplitude of 29.81 mV and an area of 2.68 mV∗s in the presence of 2.4 mmol/L extracellular Ca^{2+} (Fig. 4C, D). At this Ca^{2+} concentration, the membrane potential can be brought to about −40 mV, which is sufficient to induce rebound spikes. The robustness of RD could partly be attributed to the high density of expression of T-type Ca^{2+} channels in the soma and dendrites of thalamic relay neurons [37–39]. Third, RD can be recorded in most MGB neurons in young animals (P15–22). The prevalence of RD is in agreement with the notion that functional heterogeneous T-type Ca^{2+} channels are found in terms of pharmacological sensitivities and kinetic profiles in animals by P14 [40, 41].

HCN Channels Regulate RD Mainly by Changing the Resting Membrane Potential

HCN channels have a high level of distribution in different types of neurons in the MGB [42, 43]. Because of masking interference from Kir channels, we seldom recorded the sag phenomenon in MGB neurons. Our data demonstrated that HCN channels play an important role in the generation of RD in MGB neurons, which is consistent with previous studies in other brain regions, such as the hippocampus and superior paraolivary nucleus [7, 31]. We further showed that HCN channels regulate RD by changing the V_{rest}, because blockade of these channels hyperpolarized the V_{rest} to depress RD (Fig. 5C).

The increase in membrane resistance by blocking HCN channels (Fig. 5E) enhanced the efficiency of the hyperpolarization. Although more T-type Ca^{2+} channels were de-inactivated when the HCN channels were blocked, the hyperpolarization of the V_{rest} (offset of hyperpolarization) impeded the activation of T-type Ca^{2+} channels (Fig. 8). Besides the effects of the hyperpolarized V_{rest}, the increased input resistance did not induce a significant facilitation of RD (Fig. 5C), indicating that the increase in input resistance has little effect on RD under our conditions.

It is worth noting that there is an interaction between HCN channels and T-type Ca^{2+} channels. Activation of
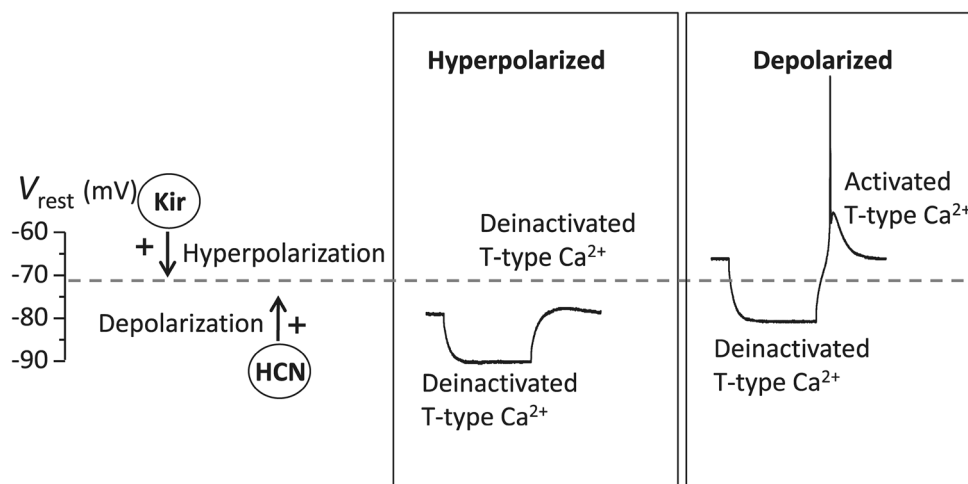

Fig. 8 Schematic showing how HCN channels and Kir channels mediate RD. Activation of HCN channels allows influx and activation of Kir channels (including GIRK channels) allows efflux of cations, which results in a depolarized or hyperpolarized membrane potential (V_{rest}). When V_{rest} is normal or depolarized, T-type Ca^{2+} channels are inactivated and are de-inactivated by a hyperpolarizing current. The offset of the hyperpolarization activates T-type Ca^{2+} channels to generate RD. When the V_{rest} is hyperpolarized, T-type Ca^{2+} channels are de-inactivated. The channels remain de-inactivated in the presence of and following offset of the hyperpolarizing current and RD is thus depressed. Dashed horizontal line indicates normal V_{rest}.

HCN channels depolarizes the membrane potential to facilitate the activation of T-type Ca^{2+} channels. In turn, the increase of intracellular Ca^{2+} induced by T-Ca^{2+} channels can increase the level of the cyclic adenosine monophosphate to upregulate the activation of HCN channels [44, 45]. This interaction plays a physiological role in the generation of burst firing in single thalamocortical neurons and the oscillatory activity of neuronal networks in the thalamus [45–50].

Kir Channels Regulate RD by Changing the Resting Membrane Potential

We showed that Kir channels play an important role in maintaining the membrane potential in MGB neurons (Fig. 6D), which is consistent with previous studies [11, 51]. We suggest that the activation of Kir channels regulates RD by both hyperpolarizing the V_{rest} and decreasing the input resistance in MGB neurons. Our results showed that blockade of Kir channels by Ba^{2+} depolarized the V_{rest} and relatively facilitated the RD in MGB neurons (Fig. 6B). Adjusting the depolarized V_{rest} to the control level did not completely recover the increased RD, indicating that the increased membrane resistance was also involved in the facilitation of RD in MGB neurons (Fig. 6C). Increased input resistance de-inactivated more T-type Ca^{2+} channels and the depolarized V_{rest} activated more of them, which manifested as a facilitation of the RD (Fig. 8).

There is a high level of expression of GIRK channels, which are one of the subfamilies of Kir channels, in MGB neurons [52–54]. Activation of GIRK channels using the $GABA_B$ receptor agonist baclofen suppressed RD (Fig. 7). Since the $GABA_B$ receptor is a G protein-coupled receptor, its activation by baclofen triggers a cascade of signals targeting a number of downstream receptors or channels, including the GIRK channel. Our results showed that the inhibitory effects of baclofen on RD were not completely reversed by blocking GIRK channels (Fig. 7B), suggesting that the activation of GIRK channels contributes to the suppression of RD but there are other possibilities. For example, $GABA_B$ receptors may mediate cyclic adenosine monophosphate synthesis to reduce the HCN current [55].

In light of the role of GIRK channels in modulating RD properties, other factors that regulate the activity of GIRK channels may also affect RD. Studies have shown that acidification, intracellular phosphatidylinositol 4,5-bisphosphate, and the concentration of Na^+ and Mg^{2+} directly influence the activation of GIRK channels [56–58]. Neurotransmitters, such as acetylcholine and 5-hydroxytryptamine, may modulate RD by activating GIRK channels [59, 60].

Functional Implications of RD in the MGB

RD, as a particular form of the postsynaptic membrane potential response to inhibitory presynaptic inputs, can transform inhibitory synaptic inputs into excitatory outputs. The MGB plays an important role in gating the transmission of auditory information [3, 61–63] and one of the obligatory functions of MGB neurons is integrating excitatory and inhibitory signals from the inferior colliculus and auditory cortex [19, 64, 65]. Thus, RD is important for MGB neurons to integrate information. Moreover, RD causes a strong Ca^{2+} influx, which gates a series of downstream Ca^{2+}-dependent activities [66, 67], such as the activation of Ca^{2+}-activated K^+ channels.

As noted above, a robust RD means activation of abundant T-type Ca^{2+} channels, which can depolarize the membrane potential. Sufficient depolarization activates voltage-dependent Na^+ channels and is expressed as rebound burst firing. RD and rebound burst firing in MGB neurons are involved in the relay and processing auditory information. First, burst firing acts as an effective relay and amplifying signal *in vivo* [68–71]. Burst firing performs better signal detection [70, 72], effectively relays auditory information in a non-linear input–output manner, regulates the frequency selectivity of MGB neurons [70, 73, 74], and may be involved in the generation of oscillations [75, 76]. Second, RD and rebound spikes may be directly responsible for neuronal off-responses [8, 77, 78], which are shown by MGB neurons [79, 80]. Although the physiological implications of off-responses are unknown, they may be associated with the direction of motion of a sound source, gap detection, and the temporal integration of duration information [8, 81, 82]. Thus, the regulatory mechanism of RD in the present study may provide a hint as to how intracellular signals modulate neuronal information processing in MGB neurons.

References

1. Grenier F, Timofeev I, Steriade M. Leading role of thalamic over cortical neurons during postinhibitory rebound excitation. Proc Natl Acad Sci U S A 1998, 95: 13929–13934.

2. Zheng N, Raman IM. Ca currents activated by spontaneous firing and synaptic disinhibition in neurons of the cerebellar nuclei. J Neurosci 2009, 29: 9826–9838.

3. Yu YQ, Xiong Y, Chan YS, He J. Corticofugal gating of auditory information in the thalamus: an in vivo intracellular recording study. J Neurosci 2004, 24: 3060–3069.

4. Hu B, Mooney DM. Burst firing induces a slow after hyperpolarization in rat auditory thalamus. Neurosci Lett 2005, 375: 162–164.

5. Bartlett EL, Smith PH. Anatomic, intrinsic, and synaptic properties of dorsal and ventral division neurons in rat medial geniculate body. J Neurophysiol 1999, 81: 1999–2016.

6. Sun H, Wu SH. Physiological characteristics of postinhibitory rebound depolarization in neurons of the rat's dorsal cortex of the inferior colliculus studied in vitro. Brain Res 2008, 1226: 70–81.

7. Felix RA, 2nd, Fridberger A, Leijon S, Berrebi AS, Magnusson AK. Sound rhythms are encoded by postinhibitory rebound spiking in the superior paraolivary nucleus. J Neurosci 2011, 31: 12566–12578.

8. Kopp-Scheinpflug C, Tozer AJ, Robinson SW, Tempel BL, Hennig MH, Forsythe ID. The sound of silence: ionic mechanisms encoding sound termination. Neuron 2011, 71: 911–925.

9. Wang X, Yu G, Hou X, Zhou J, Yang B, Zhang L. Rebound bursts in GABAergic neurons of the thalamic reticular nucleus in postnatal mice. Physiol Res 2010, 59: 273–280.

10. Tennigkeit F, Schwarz DW, Puil E. Modulation of bursts and high-threshold calcium spikes in neurons of rat auditory thalamus. Neuroscience 1998, 83: 1063–1073.

11. Tennigkeit F, Schwarz DW, Puil E. GABA(B) receptor activation changes membrane and filter properties of auditory thalamic neurons. Hear Res 1998, 122: 18–24.

12. Large EW, Crawford JD. Auditory temporal computation: interval selectivity based on post-inhibitory rebound. J Comput Neurosci 2002, 13: 125–142.

13. Casseday JH, Ehrlich D, Covey E. Neural tuning for sound duration: role of inhibitory mechanisms in the inferior colliculus. Science 1994, 264: 847–850.

14. Arcelli P, Frassoni C, Regondi MC, De Biasi S, Spreafico R. GABAergic neurons in mammalian thalamus: a marker of thalamic complexity? Brain Res Bull 1997, 42: 27–37.

15. Winer JA, Larue DT. Evolution of GABAergic circuitry in the mammalian medial geniculate body. Proc Natl Acad Sci U S A 1996, 93: 3083–3087.

16. Zhang Z, Liu CH, Yu YQ, Fujimoto K, Chan YS, He J. Corticofugal projection inhibits the auditory thalamus through the thalamic reticular nucleus. J Neurophysiol 2008, 99: 2938–2945.

17. Saint Marie RL, Stanforth DA, Jubelier EM. Substrate for rapid feedforward inhibition of the auditory forebrain. Brain Res 1997, 765: 173–176.

18. Lee CC, Sherman SM. Topography and physiology of ascending streams in the auditory tectothalamic pathway. Proc Natl Acad Sci U S A 2010, 107: 372–377.

19. Kimura A, Donishi T, Okamoto K, Tamai Y. Topography of projections from the primary and non-primary auditory cortical areas to the medial geniculate body and thalamic reticular nucleus in the rat. Neuroscience 2005, 135: 1325–1342.

20. Winer JA, Saint Marie RL, Larue DT, Oliver DL. GABAergic feedforward projections from the inferior colliculus to the medial geniculate body. Proc Natl Acad Sci U S A 1996, 93: 8005–8010.

21. Peruzzi D, Bartlett E, Smith PH, Oliver DL. A monosynaptic GABAergic input from the inferior colliculus to the medial geniculate body in rat. J Neurosci 1997, 17: 3766–3777.

22. Yu YQ, Xiong Y, Chan YS, He J. In vivo intracellular responses of the medial geniculate neurones to acoustic stimuli in anaesthetized guinea pigs. J Physiol 2004, 560: 191–205.

23. Ulrich D, Huguenard JR. GABA(A)-receptor-mediated rebound burst firing and burst shunting in thalamus. J Neurophysiol 1997, 78: 1748–1751.

24. Schwarz DW, Tennigkeit F, Adam T, Finlayson P, Puil E. Membrane properties that shape the auditory code in three nuclei of the central nervous system. J Otolaryngol 1998, 27: 311–317.

25. Luo B, Wang HT, Su YY, Wu SH, Chen L. Activation of presynaptic GABA$_B$ receptors modulates GABAergic and glutamatergic inputs to the medial geniculate body. Hear Res 2011, 280: 157–165.

26. Hibino H, Inanobe A, Furutani K, Murakami S, Findlay I, Kurachi Y. Inwardly rectifying potassium channels: their structure, function, and physiological roles. Physiol Rev 2010, 90: 291–366.

27. Quayle JM, McCarron JG, Brayden JE, Nelson MT. Inward rectifier K$^+$ currents in smooth muscle cells from rat resistance-sized cerebral arteries. Am J Physiol 1993, 265: C1363–1370.

28. Franchini L, Levi G, Visentin S. Inwardly rectifying K$^+$ channels influence Ca^{2+} entry due to nucleotide receptor activation in microglia. Cell Calcium 2004, 35: 449–459.

29. Margeta-Mitrovic M, Mitrovic I, Riley RC, Jan LY, Basbaum AI. Immunohistochemical localization of GABA(B) receptors in the rat central nervous system. J Comp Neurol 1999, 405: 299–321.

30. Padgett CL, Slesinger PA. GABA$_B$ receptor coupling to G-proteins and ion channels. Adv Pharmacol 2010, 58: 123–147.

31. Surges R, Sarvari M, Steffens M, Els T. Characterization of rebound depolarization in hippocampal neurons. Biochem Biophys Res Commun 2006, 348: 1343–1349.

32. Molineux ML, Mehaffey WH, Tadayonnejad R, Anderson D, Tennent AF, Turner RW. Ionic factors governing rebound burst phenotype in rat deep cerebellar neurons. J Neurophysiol 2008, 100: 2684–2701.

33. Tadayonnejad R, Anderson D, Molineux ML, Mehaffey WH, Jayasuriya K, Turner RW. Rebound discharge in deep cerebellar nuclear neurons in vitro. Cerebellum 2010, 9: 352–374.

34. Perez-Reyes E. Molecular physiology of low-voltage-activated T-type calcium channels. Physiol Rev 2003, 83: 117–161.

35. Carbone E, Lux HD. A low voltage-activated calcium conductance in embryonic chick sensory neurons. Biophys J 1984, 46: 413–418.

36. Huguenard JR. Low-threshold calcium currents in central nervous system neurons. Annu Rev Physiol 1996, 58: 329–348.

37. Destexhe A, Neubig M, Ulrich D, Huguenard J. Dendritic low-threshold calcium currents in thalamic relay cells. J Neurosci 1998, 18: 3574–3588.

38. Munsch T, Budde T, Pape HC. Voltage-activated intracellular calcium transients in thalamic relay cells and interneurons. Neuroreport 1997, 8: 2411–2418.

39. Errington AC, Renger JJ, Uebele VN, Crunelli V. State-dependent firing determines intrinsic dendritic Ca^{2+} signaling in thalamocortical neurons. J Neurosci 2010, 30: 14843–14853.

40. Yunker AM, McEnery MW. Low-voltage-activated ("T-Type") calcium channels in review. J Bioenerg Biomembr 2003, 35: 533–575.

41. Tarasenko AN, Kostyuk PG, Eremin AV, Isaev DS. Two types of low-voltage-activated Ca^{2+} channels in neurones of rat laterodorsal thalamic nucleus. J Physiol 1997, 499 (Pt 1): 77–86.

42. Notomi T, Shigemoto R. Immunohistochemical localization of Ih channel subunits, HCN1-4, in the rat brain. J Comp Neurol 2004, 471: 241–276.

43. Moosmang S, Biel M, Hofmann F, Ludwig A. Differential distribution of four hyperpolarization-activated cation channels in mouse brain. Biol Chem 1999, 380: 975–980.

44. Luthi A, McCormick DA. Modulation of a pacemaker current through Ca(2+)-induced stimulation of cAMP production. Nat Neurosci 1999, 2: 634–641.

45. McCormick DA, Bal T. Sleep and arousal: thalamocortical mechanisms. Annu Rev Neurosci 1997, 20: 185–215.

46. Pape HC. Queer current and pacemaker: the hyperpolarization-activated cation current in neurons. Annu Rev Physiol 1996, 58: 299–327.

26

Neurosci. Bull. February, 2016, 32(1):16–26

47. Steriade M, McCormick DA, Sejnowski TJ. Thalamocortical oscillations in the sleeping and aroused brain. Science 1993, 262: 679–685.

48. McCormick DA, Pape HC. Properties of a hyperpolarization-activated cation current and its role in rhythmic oscillation in thalamic relay neurones. J Physiol 1990, 431: 291–318.

49. Bal T, McCormick DA. What stops synchronized thalamocortical oscillations? Neuron 1996, 17: 297–308.

50. McCormick DA, Huguenard JR. A model of the electrophysiological properties of thalamocortical relay neurons. J Neurophysiol 1992, 68: 1384–1400.

51. Sutor B, Hablitz JJ. Influence of barium on rectification in rat neocortical neurons. Neurosci Lett 1993, 157: 62–66.

52. Fernandez-Alacid L, Watanabe M, Molnar E, Wickman K, Lujan R. Developmental regulation of G protein-gated inwardly-rectifying K^+ (GIRK/Kir3) channel subunits in the brain. Eur J Neurosci 2011, 34: 1724–1736.

53. Karschin C, Schreibmayer W, Dascal N, Lester H, Davidson N, Karschin A. Distribution and localization of a G protein-coupled inwardly rectifying K^+ channel in the rat. FEBS Lett 1994, 348: 139–144.

54. Ponce A, Bueno E, Kentros C, Vega-Saenz de Miera E, Chow A, Hillman D, et al. G-protein-gated inward rectifier K^+ channel proteins (GIRK1) are present in the soma and dendrites as well as in nerve terminals of specific neurons in the brain. J Neurosci 1996, 16: 1990–2001.

55. Frere SG, Luthi A. Pacemaker channels in mouse thalamocortical neurones are regulated by distinct pathways of cAMP synthesis. J Physiol 2004, 554: 111–125.

56. Mao J, Li L, McManus M, Wu J, Cui N, Jiang C. Molecular determinants for activation of G-protein-coupled inward rectifier K^+ (GIRK) channels by extracellular acidosis. J Biol Chem 2002, 277: 46166–46171.

57. Mao J, Wu J, Chen F, Wang X, Jiang C. Inhibition of G-protein-coupled inward rectifying K^+ channels by intracellular acidosis. J Biol Chem 2003, 278: 7091–7098.

58. Whorton MR, MacKinnon R. Crystal structure of the mammalian GIRK2 K^+ channel and gating regulation by G-proteins, PIP_2, and sodium. Cell 2011, 147: 199–208.

59. Mark MD, Herlitze S. G-protein mediated gating of inward-rectifier K^+ channels. Eur J Biochem 2000, 267: 5830–5836.

60. Andrade R, Malenka RC, Nicoll RA. A G protein couples serotonin and $GABA_B$ receptors to the same channels in hippocampus. Science 1986, 234: 1261–1265.

61. Zhang Y, Suga N. Corticofugal amplification of subcortical responses to single tone stimuli in the mustached bat. J Neurophysiol 1997, 78: 3489–3492.

62. Suga N, Gao E, Zhang Y, Ma X, Olsen JF. The corticofugal system for hearing: recent progress. Proc Natl Acad Sci U S A 2000, 97: 11807–11814.

63. He J. Corticofugal modulation of the auditory thalamus. Exp. Brain. Res. 2003, 153: 579–590.

64. Calford MB, Aitkin LM. Ascending projections to the medial geniculate body of the cat: evidence for multiple, parallel auditory pathways through thalamus. J Neurosci 1983, 3: 2365–2380.

65. Conley M, Kupersmith AC, Diamond IT. The organization of projections from subdivisions of the auditory cortex and thalamus to the auditory sector of the thalamic reticular nucleus in Galago. Eur J Neurosci 1991, 3: 1089–1103.

66. Cueni L, Canepari M, Lujan R, Emmenegger Y, Watanabe M, Bond CT, et al. T-type Ca^{2+} channels, SK2 channels and SERCAs gate sleep-related oscillations in thalamic dendrites. Nat Neurosci 2008, 11: 683–692.

67. Feng S, He Z, Li H, Wang Y. Ca(2+) signaling initiated by canonical transient receptor potential channels in dendritic development. Neurosci Bull 2015, 31: 351–356.

68. He J, Hu B. Differential distribution of burst and single-spike responses in auditory thalamus. J Neurophysiol 2002, 88: 2152–2156.

69. Swadlow HA, Gusev AG. The impact of 'bursting' thalamic impulses at a neocortical synapse. Nat Neurosci 2001, 4: 402–408.

70. Sherman SM. Tonic and burst firing: dual modes of thalamocortical relay. Trends Neurosci 2001, 24: 122–126.

71. Fu ZY, Mei HX, Cheng L, Bai J, Tang J, Jen PH, et al. Local neuronal circuits that may shape the discharge patterns of inferior collicular neurons. Neurosci Bull 2013, 29: 541–552.

72. Guido W, Lu SM, Sherman SM. Relative contributions of burst and tonic responses to the receptive field properties of lateral geniculate neurons in the cat. J Neurophysiol 1992, 68: 2199–2211.

73. Cotillon-Williams N, Huetz C, Hennevin E, Edeline JM. Tonotopic control of auditory thalamus frequency tuning by reticular thalamic neurons. J Neurophysiol 2008, 99: 1137–1151.

74. Massaux A, Dutrieux G, Cotillon-Williams N, Manunta Y, Edeline JM. Auditory thalamus bursts in anesthetized and non-anesthetized states: contribution to functional properties. J Neurophysiol 2004, 91: 2117–2134.

75. He J. Slow oscillation in non-lemniscal auditory thalamus. J. Neurosci. 2003, 23: 8281–8290.

76. Wallenstein GV. Simulation of $GABA_B$-receptor-mediated K^+ current in thalamocortical relay neurons: tonic firing, bursting, and oscillations. Biol Cybern 1994, 71: 271–280.

77. Takahashi H, Nakao M, Kaga K. Cortical mapping of auditory-evoked offset responses in rats. Neuroreport 2004, 15: 1565–1569.

78. Phillips DP, Hall SE, Boehnke SE. Central auditory onset responses, and temporal asymmetries in auditory perception. Hear Res 2002, 167: 192–205.

79. Aitkin LM, Prain SM. Medial geniculate body: unit responses in the awake cat. J Neurophysiol 1974, 37: 512–521.

80. He J. On and off pathways segregated at the auditory thalamus of the guinea pig. J Neurosci 2001, 21: 8672–8679.

81. Toronchuk JM, Stumpf E, Cynader MS. Auditory cortex neurons sensitive to correlates of auditory motion: underlying mechanisms. Exp. Brain Res. 1992, 88: 169–180.

82. He J, Hashikawa T, Ojima H, Kinouchi Y. Temporal integration and duration tuning in the dorsal zone of cat auditory cortex. J Neurosci 1997, 17: 2615–2625.